Establishment and Evaluation of Dual HDAC/BET Inhibitors as Therapeutic Options for Germ Cell Tumors and Other Urological Malignancies

Aaron Burmeister[1], Alexa Stephan[1], Leandro A. Alves Avelar[2], Melanie R. Müller[1], Andrea Seiwert[2], Stefan Höfmann[2], Fabian Fischer[2], Hector Torres-Gomez[2], Michèle J. Hoffmann[3], Guenter Niegisch[3,4], Felix Bremmer[5], Patrick Petzsch[6], Karl Köhrer[6], Peter Albers[4], Thomas Kurz[2], Margaretha A. Skowron[1], and Daniel Nettersheim[1]

ABSTRACT

Urological malignancies represent major challenges for clinicians, with annually rising incidences. In addition, cisplatin treatment induced long-term toxicities and the development of therapy resistance emphasize the need for novel therapeutics. In this study, we analyzed the effects of novel histone deacetylase (HDAC) and bromodomain and extraterminal domain-containing (BET) inhibitors to combine them into a potent HDAC-BET-fusion molecule and to understand their molecular mode-of-action. Treatment of (cisplatin-resistant) germ cell tumors (GCT), urothelial, renal, and prostate carcinoma cells with the HDAC, BET, and dual inhibitors decreased cell viability, induced apoptosis, and affected the cell cycle. Furthermore, a dual inhibitor considerably decreased tumor burden in GCT xenograft models. On a molecular level, correlating RNA- to ATAC-sequencing data indicated a considerable induction of gene expression, accompanied by site-specific changes of chromatin accessibility after HDAC inhibitor application. Upregulated genes could be linked to intra- and extra-cellular trafficking, cellular organization, and neuronal processes, including neuroendocrine differentiation. Regarding chromatin accessibility on a global level, an equal distribution of active or repressed DNA accessibility has been detected after HDAC inhibitor treatment, questioning the current understanding of HDAC inhibitor function. In summary, our HDAC, BET, and dual inhibitors represent a new treatment alternative for urological malignancies. Furthermore, we shed light on new molecular and epigenetic mechanisms of the tested epi-drugs, allowing for a better understanding of the underlying modes-of-action and risk assessment for the patient.

Introduction

Urological malignancies comprise different tumor entities, including germ cell tumors (GCT), prostate cancer (PC), renal cell carcinoma (RCC), and urothelial carcinoma (UC). Worldwide, new incidences of PC (3rd), UC (12th), and RCC (16th) are among the most frequent tumors of 2020 (1). GCTs are the most common tumor type of young men (14–45 years) with annually rising incidences, especially in Western countries (2).

Testicular type II GCTs arise from a precursor lesion, the "germ cell neoplasia *in situ*" (GCNIS) and can be divided into seminomas and non-seminomas. Non-seminoma, comprising embryonal carcinoma (EC) as the stem-cell like population of GCT, can further differentiate into yolk-sac tumor, teratoma, and choriocarcinoma (3). The general treatment options of GCT involve orchiectomy and subsequent chemo- or radiotherapy. Even though the treatment response is very high (above 90%), 10%–15% of patients undergo a disease relapse due to the development of cisplatin resistance. Currently, there are only limited treatment options for these patients resulting in a poor prognosis (4, 5).

Regarding UC, two thirds of patients present with a non-muscle invasive disease generally exhibiting a favorable prognosis, while the remaining present with muscle-invasive disease. Having a high risk of rapid local progression and of developing distant metastases, prognosis of the latter ones is poor and despite multimodal treatment, 5-year survival is below 50% (6, 7).

Patients with early-stage PC also display a high 10-year survival rate (93%–99%), nevertheless, castration-resistant tumors result in increased mortality (5-year survival rate of 25%; refs. 8, 9).

Treatment of non-metastatic RCCs involves surgical removal of the tumor, whereas metastatic RCC can be treated in palliative intention only by small-molecule and immune checkpoint inhibitors (10).

These challenges during treatment of urological tumors emphasize the need for a novel treatment option (11, 12).

[1]Department of Urology, Urological Research Laboratory, Translational UroOncology, Medical Faculty and University Hospital Düsseldorf, Heinrich Heine University Düsseldorf, Düsseldorf, Germany. [2]Department of Pharmaceutical and Medical Chemistry, Heinrich Heine University Düsseldorf, Düsseldorf, Germany. [3]Department of Urology, Urological Research Laboratory, Bladder Cancer Group, Medical Faculty and University Hospital Düsseldorf, Heinrich Heine University Düsseldorf, Düsseldorf, Germany. [4]Department of Urology, Medical Faculty and University Hospital Düsseldorf, Heinrich Heine University Düsseldorf, Düsseldorf, Germany. [5]Institute of Pathology, University Medical Center Goettingen, Goettingen, Germany. [6]Genomics and Transcriptomics Laboratory (GTL), Biological and Medical Research Center (BMFZ), Medical Faculty and University Hospital Düsseldorf, Heinrich Heine University Düsseldorf, Düsseldorf, Germany.

A. Burmeister, A. Stephan, and L.A. Alves Avelar contributed equally as co-authors of this article.

M.A. Skowron and D. Nettersheim contributed equally as co-authors of this article.

Corresponding Authors: Daniel Nettersheim, University Hospital Düsseldorf, Universitätsstrasse 1, 40225 Düsseldorf, Germany. Phone: 49-021-1811-5844; E-mail: Daniel.Nettersheim@med.uni-duesseldorf.de; and Margaretha A. Skowron, Margaretha.Skowron@med.uni-duesseldorf.de

Mol Cancer Ther 2022;21:1674–88

doi: 10.1158/1535-7163.MCT-22-0207

The epigenetic landscape plays a major role in the regulation of gene expression and is catalyzed by protein families of the "writers," "erasers," and "readers." The protein family of "writers" and "erasers" are direct counterparts, with the ability to add or erase post-translational histone modifications and DNA methylation marks (13). Epigenetic "readers" recognize these modifications and interpret the epigenetic code, for example, leading to recruitment of the transcription machinery (14). These epigenetic key players can be deregulated in cancer cells to circumvent cell death and are therefore a suitable target for cancer-related therapy (15).

In this study, we focused on targeting "erasers" and "readers." The inhibition of "readers," that is, bromodomain and extraterminal domain-containing (BET) proteins, such as BRD2/3/4/T has shown promising antitumor potential in breast, lung, prostate, colon, and brain cancer (16). Furthermore, the BET inhibitor (BETi) JQ1 has been studied previously in GCTs and UCs (17, 18). JQ1 induced apoptosis and a cell cycle phase accumulation, highlighting JQ1 as a potential treatment option for GCTs (17, 18).

Histone deacetylases (HDAC) belong to the epigenetic "eraser" family and several HDAC inhibitors (HDACi), for example, Romidepsin and Vorinostat, are already FDA approved as a treatment option for malignancies, such as melanoma, breast cancer, and UC (19, 20). Especially in urological malignancies, the effects of the HDACi Romidepsin have been studied intensively in GCTs and UCs (18, 21–24). In various GCT and UC cell lines, Romidepsin was able to reduce the tumor cell viability in low nanomolar concentrations via a G_2–M phase cell cycle accumulation, while inducing a radiosensitizing effect in UCs *in vivo* (22, 23). However, the major weakness of epigenetic drugs (epi-drugs) is the global effect on most cells of an organism, causing unwanted side effects, pointing out the need of less toxic novel epi-drugs. To improve efficacy and specificity of epi-drugs, combined approaches have been performed in GCTs and UCs using Romidepsin and JQ1 (17, 18). Both studies observed an improved efficacy in GCT and UC cell lines compared with single inhibitor treatment. Taking this concept a step further, the fusion of both inhibitors into a single molecule is rational, leading to improved pharmacokinetic profiles and simultaneous multiselective inhibition (25).

In this study, a library of novel HDAC and BET inhibitors has been evaluated with the goal of combining them into a single molecule, that is, an HDAC-BET-dual inhibitor, with improved epigenetic inhibition and reduced adverse effects. An HDAC-BET-dual inhibitor can present more favorable pharmacokinetics, toxicity and synergistic profiles when compared with a combination of two single compounds. Besides, the use of a single chemical entity facilitates dosage determination. Another characteristic of multitarget agents is the reduced probability of target-based drug resistance (26, 27). This may promote establishment of novel treatment options for (cisplatin-resistant) urological tumors.

Materials and Methods

Ethical statement

No ethical concerns have been risen by the ethics committee of the Medical Faculty of the Heinrich Heine University Düsseldorf (EC-HHU-D) regarding the utilization of the given cell lines for *in vitro* experiments and drug screenings (ethics votes 2018–178 and 2019–412 to D. Nettersheim). In addition, the EC-HHU-D raised no concerns on screening epi-drugs as therapeutic option for GCT *in vitro* and *in vivo* (to D. Nettersheim).

Cell culture

GCT cell lines (TCam-2, 2102EP, NCCIT, NT2/D1, 1411H, GCT-72, JAR, and JEG-3), their cisplatin-resistant sublines (-R), UC cell lines (VM-CUB-1, SCaBER, RT-112), RCC cell lines (Caki-1, 786-O, and ACHN), PC cell lines (DU-145, PC-3, and LNCaP) and the control cell lines (MPAF, HVHF2, HaCaT, JURKAT, HUVEC, and THP-1) were cultivated as described in Supplementary Table S1A and are checked for *Mycoplasma* contamination regularly. Authentications of all cell lines are available upon request (short tandem repeat analysis).

Synthesis of novel inhibitors

Two types of BRDi were synthesized, +JQ1-based (ASK series) and I-BET 762-based (PWK series) inhibitors. The synthesis of the HDAC class I/IIb (KSK64, LAK31, LAK39, LAK41 and YAK61; refs. 28–30), pan (MPK409; ref. 31), class I (K79PCHy; ref. 32), and class IIb (MPK187 and MPK377; ref. 33) inhibitors have been previously described. To evaluate the importance of class I selective inhibitors, two types of class I selective inhibitors were designed and synthesized, RGFP109-based (LAK78, LAK86, LAK88, LAK92, LAK94, LAK96, LAK98, and LAK100) and Entinostat-based inhibitors (LAK102 and LAK104). To obtain the dual inhibitors a convergent synthetic strategy was used by combining key intermediaries of the HDACi synthesis with the free acids of (+)-JQ1 or I-BET 762. Using this strategy, three dual inhibitors were synthesized, which differed in the linker between the two components: the (+)-JQ1–based hydroxamates LAK-FFK11 and LAK129, as well as the I-BET 762-based dual inhibitor LAK-HGK7. A prediction of absorption, distribution, metabolism, excretion, and toxicity (ADMET, https://admet.scbdd.com/) has been performed for the dual inhibitor LAK-FFK11 and included to the "Supplementary Materials and Methods" section (34, 35). All tested compounds possess a purity of at least 95%. HDAC assays of KSK64, LAK31, MPK409, and AlphaScreen assays of KSK64, LAK31, MPK409, ASK44, ASK58, and ASK62 have been performed by Reaction Biology. All HDACi and BETi were dissolved in DMSO. A detailed description of the drug development methodology can be found in "Supplementary Materials and Methods." A list of all used inhibitors has been included to Supplementary Table S1D.

XTT cell viability measurement

Cell viability assays have been performed as previously described (36). Briefly, $3–5\times10^3$ cells were seeded into a 96-well plate ($n = 4$). 24 hours after drug application and over a period of 4 consecutive days, 2,3-bis-(2-methoxy-4-nitro-5-sulfophenyl)-2H-tetrazolium-5-carboxanilide (XTT, 494.93 μmol/L) and phenazine methosulfate (4.2 μmol/L) were incubated for 4 hours at 37°C and measured by the iMark Absorbance Reader (Bio-Rad; absorbance: 450 nm; reference: 655 nm). EC_{50} values were calculated by GraphPad Prism v8.

Flow cytometry

As described preciously (36), apoptosis induction and cell cycle distribution were analyzed by flow cytometry by Annexin V/propidium iodide (PI) or PI-staining only, respectively, 24 hours after drug application. At least 5×10^4 cells per sample were counted by the MACSQuant Analyser 10 and the data were analyzed using MACSQuantify software v. 2.13.0 (both Miltenyi Biotec). See Supplementary Table S1B for details of antibodies used for flow cytometry.

RNA and protein isolation

RNA and proteins were extracted as previously described (36). Briefly, RNA was isolated using the, RNeasy Mini Kit according to the manufacturers protocol (Qiagen). Concentration and purity were determined by NanoDrop 2000/2000c (Thermo Fisher Scientific). Proteins were extracted by RIPA lysis buffer (Cell Signaling Technology) with 1% protease and 1% phosphatase inhibitor (Roche). Protein concentrations were quantified by the, BCA Protein Assay Kit (Thermo Fisher Scientific) according to the manufacturer's protocol.

Quantitative RT-PCR

Synthesis of complementary DNA (cDNA) and quantitative RT-PCR (qRT-PCR) were performed as previously published (36). A total of 1 μg of RNA was used for *in vitro* transcription. Gene expression was analyzed on the "384-well C1000 cycler" (Bio-Rad; $n = 3$). For data normalization, the housekeeping genes *GAPDH* and *ACTB* were used. For oligonucleotide sequences see Supplementary Table S1C.

Western blot

Western blot analysis using 20 μg of isolated proteins was performed as previously described (36). Membranes were blocked in 5% non-fat-milk in PBST (PBS + 1% Tween20) for 1 hour at RT before incubation with primary antibodies at 4°C overnight. Secondary horseradish peroxidase–conjugated antibodies were incubated for 1 hour at RT. See Supplementary Table S1B for antibody details. For imaging, the ChemiDoc Imaging System (Bio-Rad) was used.

RNA sequencing

RNA sequencing (RNA-seq) has been performed as previously described at the "Core Facility: Genomics & Transcriptomics" (Heinrich-Heine-University, Düsseldorf, Germany) using 300 ng of total RNA for mRNA capturing, fragmentation, synthesis of cDNA, adapter ligation, and library amplification (36, 37). Bead purified libraries were normalized and finally sequenced on the HiSeq 3000 System (Illumina, Inc.) with a read setup of 1×150 bp. Mapping was done against the Homo sapiens (hg38; May 25, 2017) genome sequence. Statistical differential expression tests were determined using the "Differential Expression in TWO GROUPS" tool (version 1.02; Qiagen). The resulting *P* values were corrected for multiple testing by FDR. A *P* value of ≤ 0.05 was considered significant. RNA-seq data are freely available via GEO (GSE190022).

Assay for transposase-accessible chromatin using sequencing

For ATAC-seq (assay for transposase-accessible chromatin using sequencing), 1×10^5 cells per sample were harvested 16 hours after treatment and cryopreserved for submission according to the companies' protocol and the analysis was performed by Active Motif (Active Motif) and have been publicly shared (GSE191184). A detailed description of the ATAC-seq methodology can be found in Supplementary Materials and Methods. See Supplementary Table S1D for compound details.

Xenotransplantation of GCT cells

Xenotransplantations were performed as described previously (17, 22). Briefly, 1×10^7 2102EP(-R) cells were resuspended in 500 μL Matrigel (Corning Basement Membrane; Ref. 354234) and injected into the flank of 6-weeks old male CD1 nude mice (25–30 g, Charles River Laboratories). HDACi and solvent controls were applied subcutaneously onto the xenograft using a syringe (Injekt-F Disposable 2P Injection Syringe 1 mL; Braun) every other day. Animal experiments were conducted according to the German law of animal protection and in agreement with the approval of the local institutional animal care committees (Landesamt für Natur, Umwelt und Verbraucherschutz NRW; AZ 81-02.04.2018.A350). Tissue samples were counterstained with Meyer's hematoxylin (Dako, Agilent Technologies) on 2-μm FFPE xenografts tissue sections for 8 min, and analyzed by the use of light microscopy, as described previously (38).

(Online) analysis tools and software

RNA-seq gene expression data of urological cell lines from "Cancer Cell Line Encyclopedia" (CCLE) were analyzed by "UCSC Xena browser" (https://xena.ucsc.edu; ref. 39). Gene alterations/mutations of urological malignancies from "The Cancer Genome Atlas" (TCGA) dataset were analyzed by "cBioPortal" (https://www.cbioportal.org/; refs. 40, 41). Venn diagrams were created by "InteractiVenn" (http://www.interactivenn.net; ref. 42). To predict gene interactions, the STRING algorithm was used (https://string-db.org; ref. 43). DAVID was used to perform functional annotation (https://david.ncifcrf.gov/home.jsp; ref. 44). The HOMER algorithm was used to screen for affected transcription factor binding motifs after HDACi application (45). Circos diagrams were created by "shinycircos" (46), PCA (principal component analysis) were designed with PCAGO (47). "Python" was used to generate volcano plots (48, 49). Prognostic marker data for *KIRREL* and *MARVELD1* were taken from the "The Human Protein Atlas" (https://www.proteinatlas.org; ref. 50). Figures contain graphics from BioRender (https://biorender.com).

Statistical analysis

To analyze differences between groups, two-tailed Student *t* tests after confirming equality of two variances according to the F-test have been performed. Statistically significant differences were highlighted by asterisk (*, $P < 0.05$).

Data availability

The data generated in this study are publicly available in Gene Expression Omnibus (GEO) at GSE190022 and GSE191184.

Results

Screening the expression of different members of the HDAC classes and BET protein family demonstrated high expression of HDAC class I and IIb in UC, RCC, PC, and GCT (Supplementary Fig. S1A and S1B). There were no HDAC and BET mutations reported in GCTs, whereas UC and PC acquired missense and fusion mutations, especially in *HDAC1/2/4* and in *BRD2/4* genes Supplementary Fig. S1C). Analysis of RCCs showed rare missense mutations in *HDAC1/6/8* and in *BRD1/2*. On the basis of high expression levels in urological malignancies, we focused on inhibitors targeting HDAC class I/IIb and BRD2 (Supplementary Fig. S1).

A screening of 18 novel HDACi and 15 BETi in GCT cell lines (seminoma: TCam-2, EC: 2102EP, CC: JAR), as well as in VM-CUB-1 (UC), Caki-1 (RCC), and DU-145 (PC) revealed that 20 (13 HDAC and 7 BET inhibitors) drugs considerably reduced cell viability at micromolar concentrations (1–10 μmol/L; Supplementary Fig. S2, Supplementary Data S1A and S1B). On the basis of this initial screening, three potent HDACi (KSK64, LAK31, and MPK409) and BETi (ASK44, ASK58, and ASK62) were further characterized in this study.

We determined the specificity for the target molecules of the HDACi and BETi by enzyme assays (Supplementary Figs. S3A

and S3B, S4A and S4B; ref. 30). KSK64, LAK31, and MPK490 showed a high affinity toward HDAC1/2/3/6 (EC_{50} 1–100 nmol/L; Supplementary Figs. S3A and S4A). For comparison, we included literature data of the structural similar HDACi Entinostat, which inhibits HDAC1 (EC_{50} 300 nmol/L) over HDAC3 (EC_{50} 8 μmol/L), while not targeting HDAC8 (51). The three BETi targeted mainly BRD2 (EC_{50} 50–200 nmol/L) and to a lower extent BRD3/4/T (Supplementary Figs. S3B and S4B). In contrast, JQ1 predominantly targeted BRD4 and BRD2 (Supplementary Fig. S4B; ref. 14). An increased pan-histone 3-acetylation (pan-H3ac) after 16 hours of HDACi treatment was verified in all four tumor entities via western blotting (Supplementary Fig. S4C).

An extensive analysis in 22 tumor (GCT, UC, RCC, and PC) and 6 control cell lines (fibroblasts, keratinocytes, T-lymphocytes, endothelial cells, and monocytes) validated the reduction in cell viability in cancer cell lines upon treatment with the HDACi or BETi (EC_{50} mean: KSK64: 1.1 μmol/L; LAK31: 1.1 μmol/L; MPK409: 1.3 μmol/L; ASK44: 6.6 μmol/L; ASK58: 6.9 μmol/L and ASK62: 6.3 μmol/L), whereas non-cancerous fibroblast cells and keratinocytes were less affected (**Fig. 1A** and **B**; Supplementary Data S1C and S1D). Immune cells (JURKAT T-lymphocytes, THP-1 monocytes) and endothelial cells (HUVEC) responded at similar HDACi/BETi concentrations as GCT cells (**Fig. 1A** and **B**). In direct comparison with structurally similar drugs, such as Entinostat, Vorinostat (HDACi) and JQ1 (BETi), the novel epi-drugs reduced the cell viability at lower concentrations (**Fig. 1A**).

To evaluate, whether the reduction in cell viability was attributed to induction of apoptosis or cell cycle phase accumulation, we performed flow cytometry analysis (**Fig. 1C** and **D**; Supplementary Data S1E). Already 24 hours after treatment (EC_{50} 48 hours) with the three most potent HDACi or BETi, an induction of apoptosis (>5%) could be detected in most GCT cell lines, including cisplatin-resistant subclones (-R; **Fig. 1C**). Caki-1 cells (RCC) remained nearly unaffected upon treatment with both, HDACi or BETi (**Fig. 1C**). In other cancer cell lines, such as VM-CUB-1 (UC) and DU-145 (PC) treatment with all three HDACi induced apoptosis compared with the solvent control (**Fig. 1C**). In general, the HDACi were more potent than the BETi in inducing apoptosis (**Fig. 1C**). At used concentrations, the HDACi and BETi did not affect viability of fibroblasts (MPAF; **Fig. 1C**). To confirm apoptosis induction, GCT cells TCam-2, 2102EP, and JAR were treated with the HDACi LAK31 as well as the BETi ASK44 and subsequent western blot analysis revealed cleavage of PARP (Supplementary Fig. S4D).

Our analysis of the cell cycle phase distribution after HDACi treatment demonstrated a cell line–dependent accumulation in either the G_1–G_0 or the G_2–M phase. The GCT cell lines NT2/D1(-R), JAR and JEG-3-R, as well as the VM-CUB-1 (UC) accumulated in the G_1–G_0 phase. In contrast, the GCT cell lines TCam-2-R, 2102EP-R, 1411H and JEG-3, as well as Caki-1 (RCC) and DU-145 (PC) accumulated in the G_2–M phase. Compared with the solvent control, the BETi mainly induced accumulation in G_1–G_0 phase in most cancer cell lines. The BETi did not affect the cell cycle of fibroblasts, whereas the HDACi induced a G_2–M phase accumulation (**Fig. 1D**). Thus, in cancer cells the novel inhibitors induced apoptosis already 24 hours after a single drug application, accompanied by a cell cycle phase accumulation in the G_1–G_0 or the G_2–M phase.

Next, we aimed at deciphering the molecular and epigenetic mode of action of each tested epi-drug. By ATAC-sequencing (ATAC-seq), we evaluated whether there were alterations in chromatin accessibility upon treatment with the HDACi LAK31, allowing us to further characterize global as well as site-specific effects. First, we validated that LAK31 treatment increased pan-H3ac in cell lines of urological malignancies (Supplementary Fig. S4C and S4D). Then, we performed an ATAC-seq in four tumor cell lines representing the different urological cancer entities (2102EP, VM-CUB-1, Caki-1, and DU-145) and compared LAK31 treatment with solvent controls (Supplementary Data S2A–S2G). Only normalized tag counts were analyzed, leading to identification of 224,159 merged peak regions (Supplementary Figs. S5A, S5B, and S6A). A Pearson's correlation coefficient matrix was used to illustrate and compare changes in chromatin accessibility between the analyzed samples (Supplementary Fig. S5C). Changes in chromatin accessibility in gene bodies, promotors, and merged peak regions after LAK31 treatment are shown in Supplementary Fig. S5D. By a circos diagram, we illustrated changes in genome-wide accessibility, demonstrating an equal distribution of elevated or diminished DNA accessibility after LAK31 treatment (Supplementary Fig. S6B and S6C). A PCA demonstrated a clear shift of LAK31 treated samples apart from their solvent controls (**Fig. 2A**). A bar plot summarizing the total number of differentially altered regions [fold change (FC) > 2] confirmed a parallel opening and closing of chromatin on a global level (**Fig. 2B**).

To exclude that these observations were specifically caused by our novel epi-drugs, we performed ATAC-seq of 2102EP cells treated with the established HDACi Romidepsin and Quisinostat (Supplementary Data S2B and S2C; Supplementary Figs. S5 and S6A, S6C). As a "negative control," we included an inhibitor of an epigenetic "reader" (MZ-1, a PROTAC targeting BRD4; Supplementary Data S2D; Supplementary Figs. S5 and S6A, S6C). Both, Romidepsin and Quisinostat treated 2102EP cells, showed a similar DNA accessibility profile as LAK31 treated cell lines of urological malignancies, whereas effects of MZ-1 on DNA accessibility were negligible (**Fig. 2C** and **D**). In 2102EP cells, we identified transcription factor–binding motifs in regions altered in DNA accessibility after HDACi (LAK31, Quisinostat, Romidepsin) treatment by the HOMER algorithm (**Fig. 2E**, Supplementary Data S2H). A considerable overlap between the HDACi regarding the identified TOP50 motifs has been found (41 shared motifs in accessible DNA and 35 in inaccessible DNA; **Fig. 2E**). Among the motifs linked to accessible DNA, FOS- (FOSL2, FRA1/2) and ATF3-related motifs were identified, which is in line with upregulation of both factors after HDACi treatment (22). Among the motifs linked to inaccessible DNA, chromatin-remodelers and -modifiers CTCF and CTCFL (BORIS) as well as pluripotency factors like OCT4 and SOX2 were identified, which is in line with downregulation of pluripotency factors after HDACi treatment (**Fig. 2E**; refs. 22, 52). To further decipher the molecular mode of action of HDACi, RNA-seq has been performed with LAK31 treated cells of each tumor entity (GCT: 2102EP, UC: VM-CUB-1, RCC: Caki-1, PC: DU-145). Volcano plots of deregulated transcripts ($P \leq 0.05$, FC $\geq \pm \log_2 2$) after LAK31 treatment in comparison with solvent controls (DMSO) showed a strong increase in transcription after HDAC inhibition (2102EP: 2526 genes; VM-CUB-1: 4948 genes; Caki-1: 4103 genes; DU-145: 3010 genes; **Fig. 3A**; Supplementary Data S2I–S2L). A three-dimensional PCA indicated a clear separation of the solvent control from HDACi treated cells (**Fig. 3B**). A gene ontology analysis of 190 commonly upregulated genes in all four tumor entities after HDAC inhibition (Supplementary Data S2M) identified factors involved in "extracellular matrix," "intra- and extracellular membrane-associated trafficking and cell–cell communication," and "intracellular trafficking and cytoskeleton," "cilium" and "cell projection" associated genes, "neuronal associated factors" and "protein features"

A

Tumor entity			Cell line	HDACi					BETi			
				Entinostat	Vorinostat	KSK64	LAK31	MPK409	JQ1	ASK44	ASK58	ASK62
GCT	Seminoma		TCam-2	2.4	0.2	1.2	0.5	0.6	>5	>10	>10	>10
			TCam-2-R	>10	0.2	0.6	0.6	0.6	2.4	>10	>10	5.6
	Non-seminoma	EC	2102EP	1.9	>10	0.2	0.2	0.2	>5	2.4	9.5	4.1
			2102EP-R	3.5	1.8	0.2	0.3	0.3	>5	>10	>10	8.1
			NCCIT	2.9	0.4	0.6	0.6	0.7	0.1	0.3	0.2	0.4
			NCCIT-R	2.3	1.0	0.6	0.6	0.7	1.0	3.3	8.4	5.4
			NT2/D1	4.1	0.3	0.6	0.5	0.7	0.1	0.3	0.4	0.7
			NT2/D1-R	3.1	2.9	0.3	0.3	0.3	1.8	1.3	0.6	1.1
		YST	1411H	3.9	1.2	0.4	0.4	0.6	>5	>10	>10	>10
			GCT-72	1.1	0.4	0.1	0.3	0.4	>5	8.1	4.9	7.9
		CC	JAR	4.6	1.4	0.9	0.5	1.0	>5	>10	>10	>10
			JEG-3	3.8	1.6	0.8	0.7	1.0	>5	>10	>10	>10
			JEG-3-R	3.6	1.2	0.9	0.7	0.9	>5	>10	>10	>10
UC			VM-CUB-1	5.9	4.0	1.2	1.2	2.1	0.3	1.4	1.5	1.6
			SCaBER	>10	5.9	2.3	1.5	1.8	1.5	>10	>10	>10
			RT-112	>10	5.4	2.4	2.6	3.7	>10	>10	>10	>10
RCC			Caki-1	>10	3.3	2.0	2.5	3.3	>10	5.3	5.3	3.3
			786-O	>10	>10	2.5	5.0	3.2	>10	>10	>10	>10
			ACHN	>10	7.1	1.7	2.4	2.8	2.8	2.7	4.5	2.9
PC			DU-145	1.4	3.0	0.8	0.7	0.7	>10	>10	>10	>10
			PC-3	8.5	8.3	2.2	1.9	2.8	3.8	>10	5.1	6.5
			LNCaP	1.0	2.0	0.6	1.0	0.8	0.2	1.3	1.1	1.5

LD_{50} 48h 0.5 µmol/L 0.5 µmol/L 10 µmol/L

B

Control cell lines		HDACi				BETi			
		Entinostat	KSK64	LAK31	MPK409	JQ1	ASK44	ASK58	ASK62
Fibroblasts	MPAF	>10	>10	>10	>10	>5	>10	>10	>10
	HVHF2	>10	4.2	9.1	9.8	>5	>10	>10	>10
Keratinocytes	HaCaT	8.3	1.3	1.4	1.2	>5	>10	>10	>10
Endothelial cells	HUVEC	6.8	<0.5	0.7	0.7	4.0	<2	<2	4.6
T-lymphocytes	JURKAT	<0.5	<0.5	<0.5	<0.5	2.4	4.2	6.7	3.7
Monocytes	THP-1	1.3	<0.5	<0.5	0.5	<2	<2	<2	<2

LD_{50} 48h 0.5 µmol/L 0.5 µmol/L 10 µmol/L

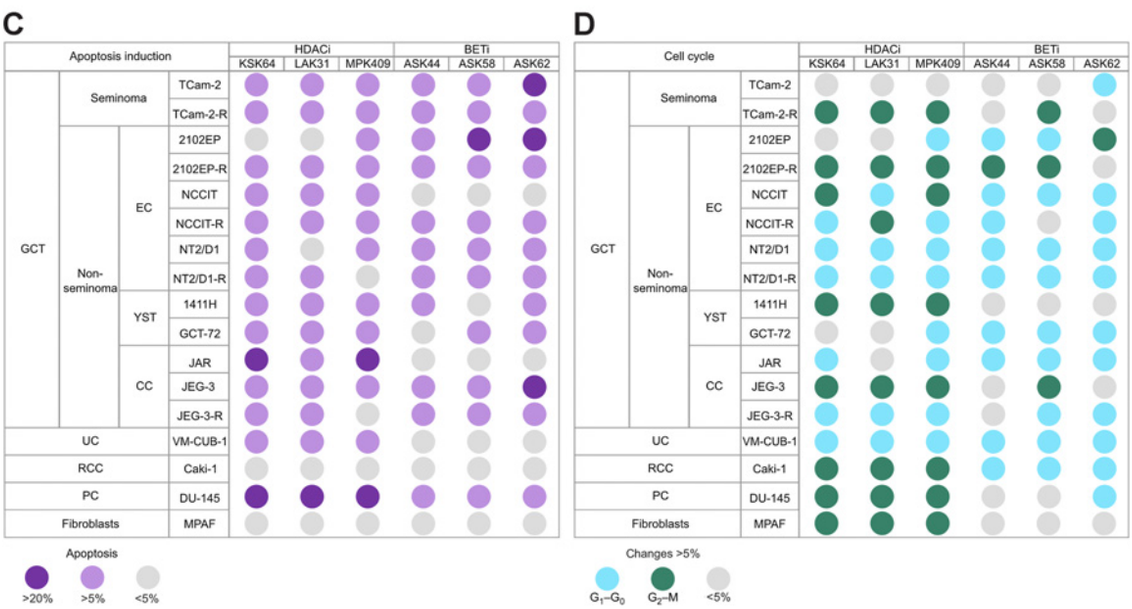

Figure 1.

Screening for cytotoxicity of the novel HDAC and BET inhibitors in urological malignancies. Illustration of the micromolar EC_{50} values acquired by XTT cell viability assays 48 hours after treatment of urological malignancies (**A**) or healthy untransformed cells (**B**) with HDACi and BETi. The HDACi Entinostat and Vorinostat were compared with the three novel HDACi inhibitors KSK64, LAK31, and MPK409, whereas JQ1 was compared with the novel BETi ASK44, ASK58, and ASK62. A red color code indicates high EC_{50} values (> 5 µmol/L), whereas green tiles represent a low EC_{50} (< 2 µmol/L). The inhibitors were analyzed in cell lines of all four tumor entities (UC, RCC, PC, and GCT). For GCTs cisplatin-resistant cell lines (-R) were also included. Color-coded flow cytometry-based analysis of apoptosis induction (**C**) and cell-cycle phase distribution (**D**) 24 hours after EC_{50} treatment of HDACi/BETi in cell lines of all four tumor entities (UC, RCC, PC, and GCT) in comparison with a DMSO solvent control.

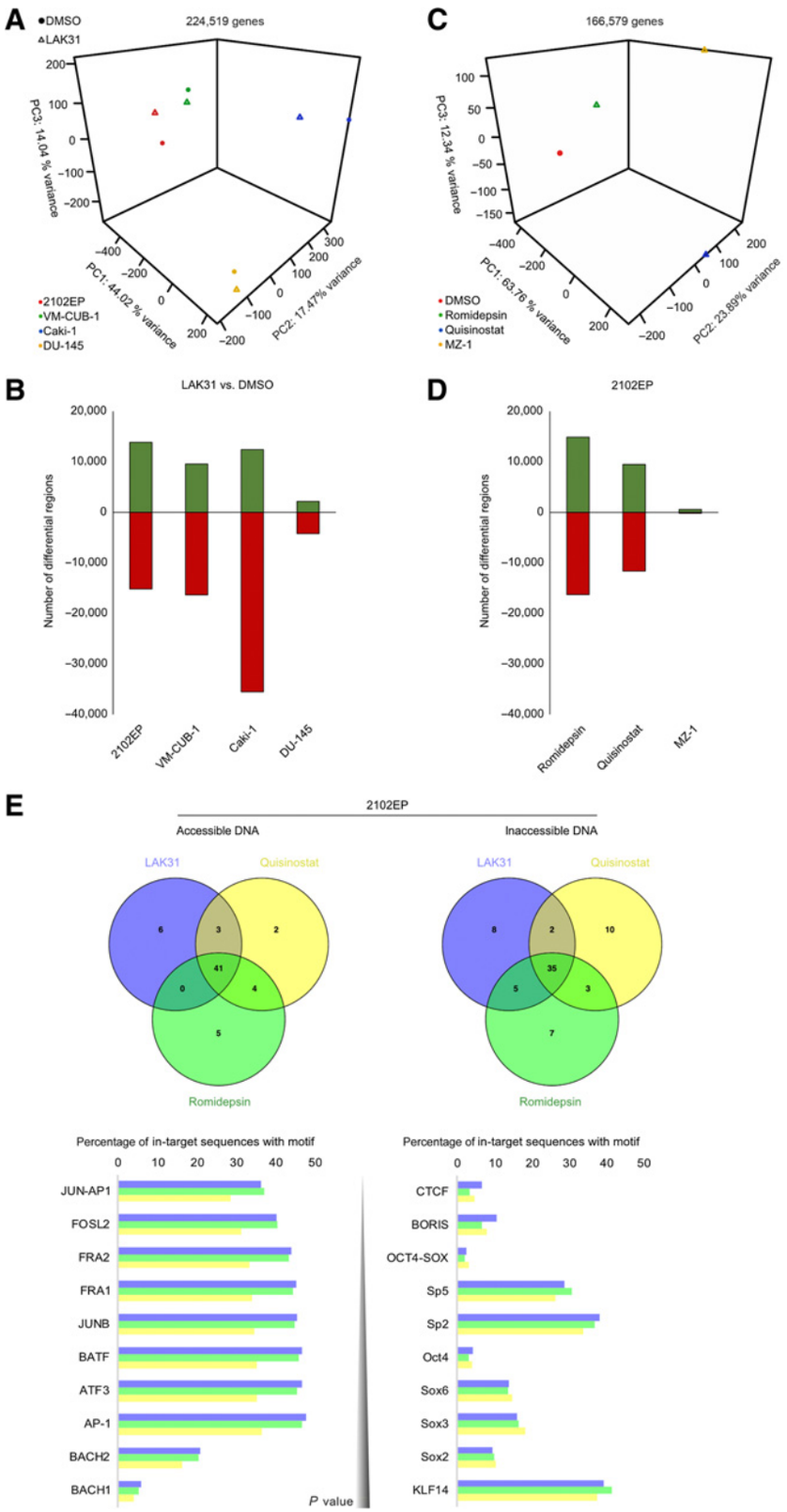

Figure 2.

Analysis of global changes of chromatin accessibility after LAK31 treatment in four different urological tumor entities. **A,** A PCA of LAK31-induced changes (triangles) in chromatin accessibility in cell lines of all four tumor entities in comparison with DMSO solvent control (spheres). **B,** A bar plot illustrating the number of opened (green) and closed (red) chromatin regions after LAK31 treatment in 2102EP, VM-CUB-1, Caki-1, and DU-145 in comparison with DMSO solvent control. **C,** A PCA of HDACi-induced changes (triangles; romidepsin, quisinostat, MZ-1) in chromatin accessibility in 2102EP cells in comparison with DMSO solvent control (sphere). **D,** A bar plot illustrating the number of opened (green) and closed (red) chromatin regions after Romidepsin, Quisinostat, or MZ-1 treatment in 2102EP cells in comparison with DMSO solvent control. **E,** A HOMER algorithm-based screening for transcription factor–binding motifs in DNA rendered accessible or inaccessible after HDACi treatment of 2102EP cells. Venn diagrams summarize similarities in the identified TOP50 motifs. Bar diagrams highlight the TOP10-binding motifs (sorted by *P* value in LAK31 treated 2102EP cells) and their distribution in target sequences affected by HDACi treatment.

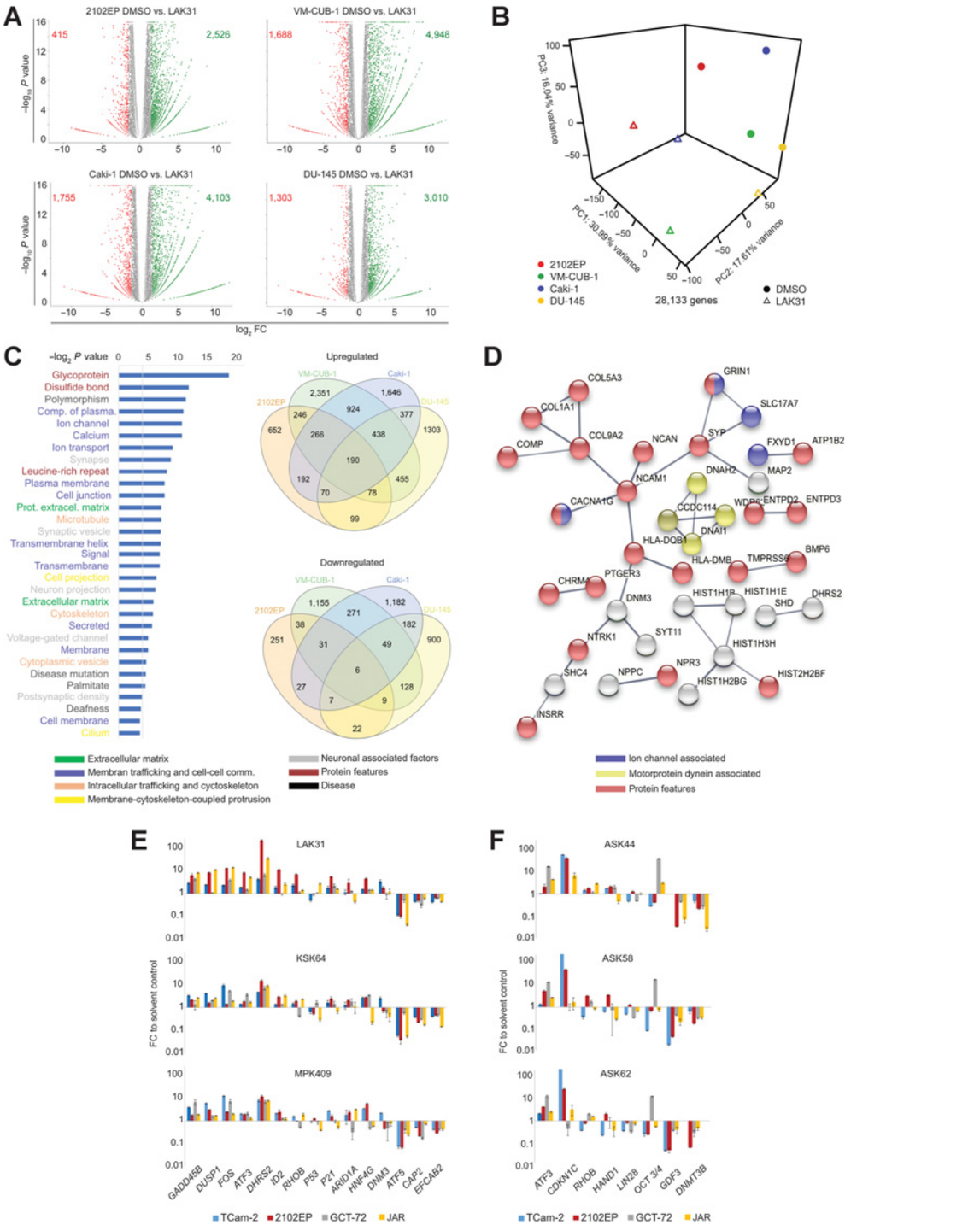

Figure 3.

Deciphering of the molecular processes induced by HDACi LAK31 in urological malignancies. **A,** Volcano plots of transcriptional changes upon LAK31 treatment in comparison with the DMSO solvent control in 2102EP, VM-CUB-1, Caki-1, and DU-145, acquired by RNA-seq (FC < $-\log_2 2$ is shown in red; FC > $\log_2 2$ is shown in green). The number of up- /downregulated genes is given in each plot. **B,** A PCA illustrating the changes in transcription upon LAK31 treatment in comparison with the DMSO control. **C,** DAVID analysis and Venn diagrams for commonly up- and downregulated genes of cell lines of all four tumor entities (2102EP, VM-CUB-1, Caki-1, and DU-145) after LAK31 treatment. 190 genes were commonly upregulated (FC > $\log_2 2$), whereas 6 were commonly downregulated (FC < $-\log_2 2$) . **D,** STRING interaction analysis of commonly upregulated genes in 2102EP, VM-CUB-1, Caki-1, and DU-145 upon LAK31 treatment compared with the solvent control. **E,** qRT-PCR validation gene expression panel of the three most potent novel HDACi (KSK64, LAK31, and MPK409) in GCT cell lines TCam-2 (blue), 2102EP (red), GCT-72 (gray), and JAR (yellow). **F,** qRT-PCR analysis of a gene expression panel of key players of BETi in GCT cell lines treated with the three most potent novel BETi (ASK44, ASK58, and ASK62).

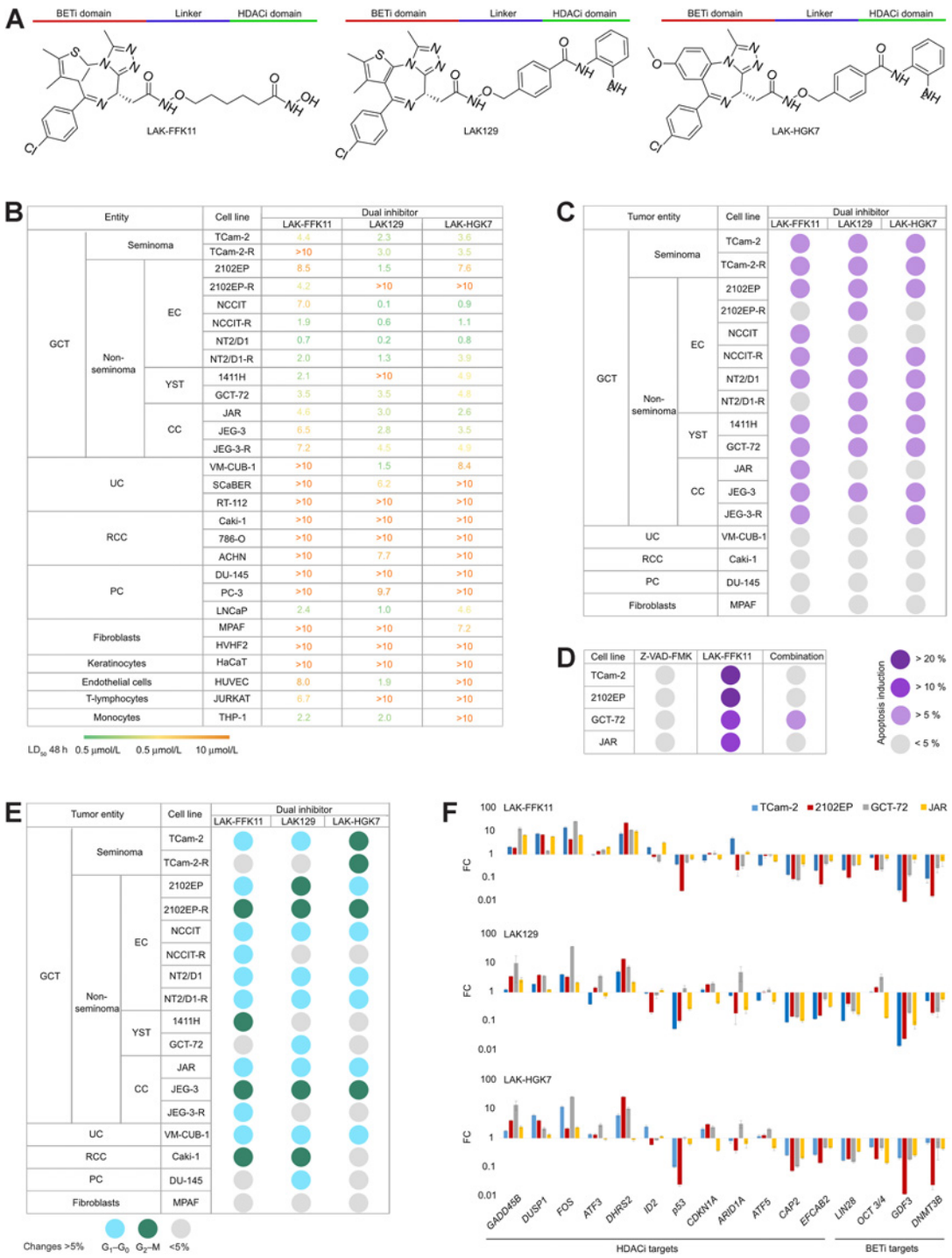

Figure 4.

Characterization of novel HDAC-BET-dual inhibitors. **A,** Structures of the three novel HDAC-BET-dual inhibitors (LAK-FFK11, LAK129, and LAK-HGK7). **B,** Illustrations of the micromolar EC_{50} values 48 hours after treatment with HDAC-BET-dual inhibitors as acquired by XTT cell viability assays. A red color code indicates high EC_{50} values (> 5 µmol/L), whereas green tiles represent a low EC_{50} (< 2 µmol/L). The inhibitors were analyzed in cell lines of all four tumor entities (UC, RCC, PC, and GCT) and six healthy control cell lines. For GCTs cisplatin-resistant cell lines (-R) were also included. **C,** Color-coded flow cytometry-based analysis of apoptosis rates 24 hours after EC_{50} application of dual inhibitors in cell lines of all four tumor entities (UC, RCC, PC, and GCT) in comparison with the DMSO solvent control and (**D**) upon co-treatment with the caspase-inhibitor Z-VAD-FMK. **E,** Color-coded flow cytometry-based analysis of cell cycle phase distribution 24 hours after EC_{50} application of dual inhibitors in cell lines of all four tumor entities (UC, RCC, PC, and GCT) in comparison with the DMSO solvent control. **F,** A qRT-PCR analysis of expression of key players of HDACi and BETi.

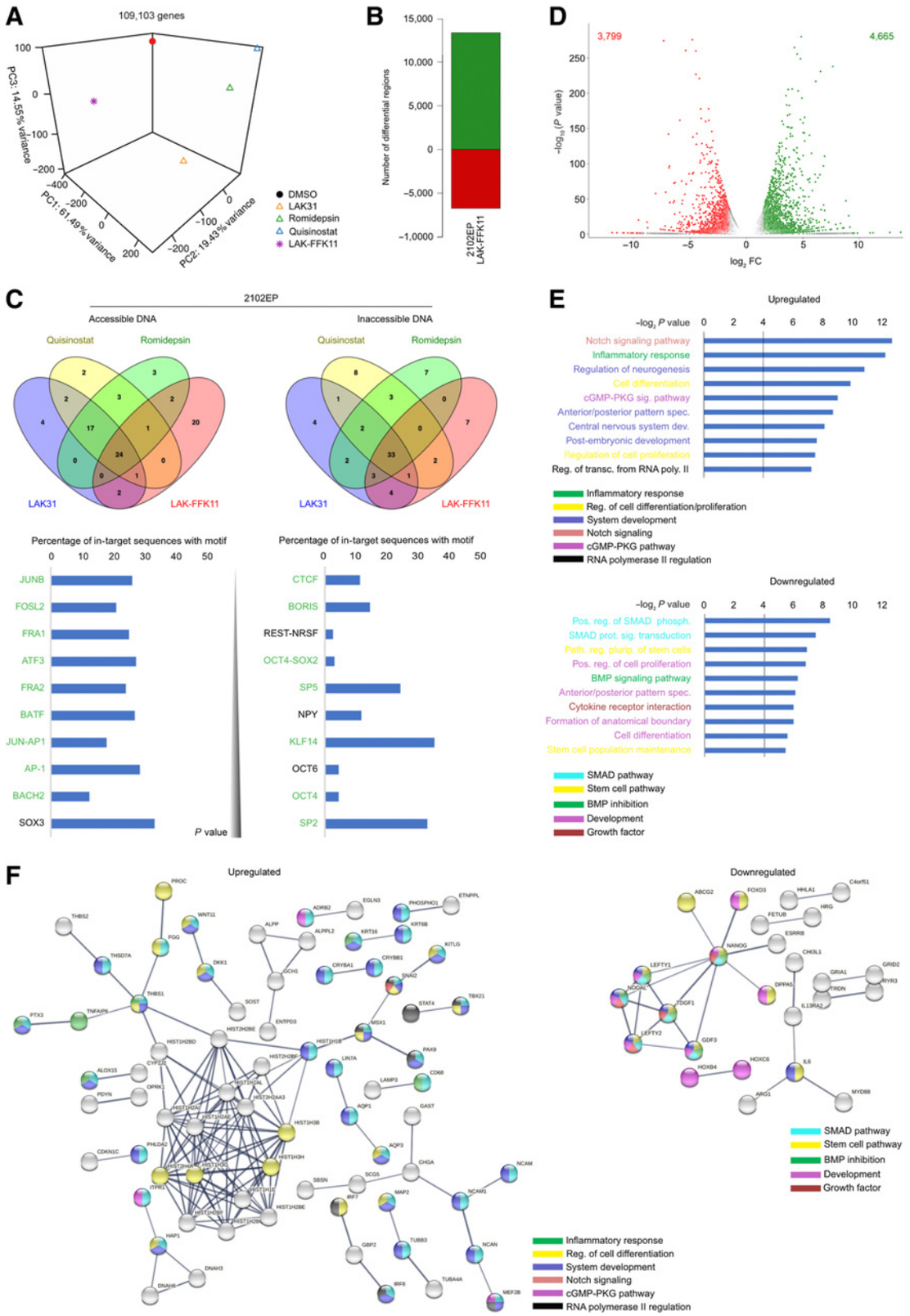
A
109,103 genes
PC3: 14.55% variance
PC1: 61.49% variance
PC2: 19.43% variance
DMSO
LAK31
Romidepsin
Quisinostat
LAK-FFK11
B
Number of differential regions
2102EP
LAK-FFK11
D
3,799
4,665
−log10 (P value)
log2 FC
C
2102EP
Accessible DNA
Inaccessible DNA
Quisinostat
Romidepsin
LAK31
LAK-FFK11
Percentage of in-target sequences with motif
JUNB
FOSL2
FRA1
ATF3
FRA2
BATF
JUN-AP1
AP-1
BACH2
SOX3
P value
CTCF
BORIS
REST-NRSF
OCT4-SOX2
SP5
NPY
KLF14
OCT6
OCT4
SP2
E
Upregulated
−log2 P value
Notch signaling pathway
Inflammatory response
Regulation of neurogenesis
Cell differentiation
cGMP-PKG sig. pathway
Anterior/posterior pattern spec.
Central nervous system dev.
Post-embryonic development
Regulation of cell proliferation
Reg. of transc. from RNA poly. II
Inflammatory response
Reg. of cell differentiation/proliferation
System development
Notch signaling
cGMP-PKG pathway
RNA polymerase II regulation
Downregulated
Pos. reg. of SMAD phosph.
SMAD prot. sig. transduction
Path. reg. plurip. of stem cells
Pos. reg. of cell proliferation
BMP signaling pathway
Anterior/posterior pattern spec.
Cytokine receptor interaction
Formation of anatomical boundary
Cell differentiation
Stem cell population maintenance
SMAD pathway
Stem cell pathway
BMP inhibition
Development
Growth factor
F
Upregulated
Downregulated
SMAD pathway
Stem cell pathway
BMP inhibition
Development
Growth factor
Inflammatory response
Reg. of cell differentiation
System development
Notch signaling
cGMP-PKG pathway
RNA polymerase II regulation

(i.e., "glycoproteins," "disulfide bond"). Via the STRING algorithm, we predicted interaction of the commonly upregulated genes (FC ≥ $\pm\log_2 2$; **Fig. 3C**). The network included genes coding for histones (i.e., *HIST1H1B/H1E/H3H*), as well as another smaller network that could be associated with the motor protein dynein of sperm flagella (i.e., *DNAH2/I1*; **Fig. 3D**). The largest network displayed a connection between genes encoding for collagen (*COL9A2/5A3/1A1)* and ion channel associated genes (*CACNA1G*, *GRIN1*, and *SLC17A7*; **Fig. 3D**). A STRING analysis predicted interaction of all genes related to neuronal differentiation and development (Supplementary Fig. S7A). Only six genes were commonly downregulated in all four tumor entities, here STRING did not detect any interactions.

To validate the RNA-seq data, we performed qRT-PCR analysis in GCT cell lines (**Fig. 3E** and **F**) as well as UC, PC, and RCC cell lines (Supplementary Fig. S7B) after application of three HDACi (LAK31, KSK64, and MPK409). In addition, we included genes known to be deregulated by the HDACi Romidepsin and Vorinostat (**Fig. 3E** and **F**; Supplementary Fig. S7B and S7C; refs. 22, 53). The HDACi LAK31, KSK64, and MPK409 induced similar deregulations in gene expression as Romidepsin and Vorinostat, with an upregulation of stress response factors as well as apoptosis and cell cycle regulators (*ATF3, CDKN1A, DHRS2, DUSP1*, *FOS*, and *GADD45B*) and downregulation of *ATF5*, *CAP2*, and *EFCAB2* (**Fig. 3E**; Supplementary Fig. S7B; ref. 22).

Because the new BETi ASK44, ASK58, and ASK62 are analogues of JQ1, we screened previously described JQ1 effectors in GCT cell lines (**Fig. 3F**; ref. 17). The three BETi induced similar deregulations in gene expression as JQ1, like upregulation of stress response and cell cycle regulators (*ATF3* and *CDKN1C*) and downregulation of *DNMT3B* and *GDF3*.

By correlating ATAC- to RNA-seq data, we identified locus-specific changes of chromatin accessibility and transcription (Supplementary Data S2N–S2Q). We summarized all genes commonly up- or downregulated in expression and correlating the according DNA accessibility between the different tumor cell lines in Supplementary Data S2R–S2S. VM-CUB-1 (UC) and Caki-1 (RCC) showed the highest overlap in deregulated genes (66 upregulated / DNA accessible; 116 downregulated/DNA inaccessible), whereas DU-145 (PC) showed only few overlapping factors, which might be due to the overall weak alterations caused by LAK31 in these cells (Supplementary Fig. S7D; Supplementary Data S2R–S2S). Among all tumor cell lines, we found *TEX14* (*Testis Expressed 14;* necessary for intercellular bridges in germ cells required for spermatogenesis) to be commonly upregulated in expression and affected by DNA accessibility, whereas *KIRREL* (*Kirre Like Nephrin Family Adhesion Molecule 1, NEPH1*; fully transactivates the transcription factor AP-1 in presence of TEC kinases) and *MARVELD1* (*MARVEL Domain Containing 1;* a microtubule-associated gene, inhibits proliferation and migration) were downregulated in expression and correlated to diminished DNA accessibility at corresponding loci (Supplementary Fig. S7D and S7E; Supplementary Data S2R–S2S). On the basis of these results, dual inhibitors were designed and synthesized (Supplementary Materials and Methods). Each fusion molecule consists of a BETi component coupled to an HDACi domain via a linker (**Fig. 4A**). First, LAK-FFK11 had been synthesized, in which the BETi domain replaces the CAP-domain of the HDACi (**Fig. 4A**). Furthermore, a second and third fusion molecule had been synthesized (LAK129 and LAK-HGK7), where we kept the HDACi CAP group and conjugated the BET inhibitor domain directly onto the CAP group (**Fig. 4A**). Enzymatic assays revealed a high affinity of LAK-FFK11 toward BRD2/3/4/T in a low nanomolar range and toward HDAC1/3/6 in high nanomolar range (Supplementary Fig. S4E and S4F). A western blot analysis verified an increased pan-H3ac after 16 hours of dual inhibitor treatment in GCT cell lines (TCam-2, 2102EP, and JAR; Supplementary Fig. S4G). In addition, because the BET inhibitor JQ1 has been shown to decrease the chromatin accessibility in gastric cancer cells (54), pan-H3ac upon treatment with the most promising dual inhibitor LAK-FFK11 has been compared with the HDACi LAK31 and BETi ASK44 in TCam-2, 2102EP, and JAR cells (Supplementary Fig. S4D). As such, enhanced pan-H3ac has been noted in both, LAK31 or LAK-FFK11–treated cells, thereby affirming that the BETi-component of the dual inhibitor did not counteract histone acetylation.

An *in silico* prediction of absorption, distribution, metabolism, excretion, and toxicity (ADMET) of the HDAC-BET-dual inhibitor LAK-FFK11 indicated that the drug should be well absorbed, distributed and metabolized (Supplementary Materials and Methods). Though, the ADMET prediction might indicate a fast clearance of the drug and possible hepatoxicity should be further evaluated in future studies (Supplementary Materials and Methods).

By XTT assays, we screened for the potential of the dual inhibitors to kill urological cancer cells. The EC_{50} values of the tested dual inhibitors ranged from 0.1 to 10 μmol/L in GCT cell lines, with the highest efficacy in EC cell lines (**Fig. 4B**; Supplementary Data S1C and S1D). The dual inhibitors were not as effective as in GCT cells in most UC (SCaBER, RT-112), RCC (Caki-1, 786-O, and ACHN) and PC (DU-145 and PC-3) cell lines, except VM-CUB-1 and LNCaP (**Fig. 4B**; Supplementary Data S1C and S1D). Healthy control cell lines (fibroblasts: MPAF and HVHF2; keratinocytes: HaCaT; T lymphocytes: JURKAT; endothelial cells: HUVEC) were less affected by the dual inhibitors, than GCT cell lines (**Fig. 4B**).

In comparison with the solvent controls, the flow cytometric analysis as well as PARP cleavage confirmed increased apoptosis in most GCT cell lines upon treatment with the dual inhibitors (**Fig. 4C**; Supplementary Fig. S4G, Supplementary Data S1E). To validate the caspase-dependent apoptosis induction, GCT cells have been simultaneously treated with the dual inhibitor and the caspase inhibitor Z-VAD-FMK. As such, apoptosis induction could be reverted in GCT cells, thereby confirming induction of the caspase-dependent apoptotic cascade by the dual inhibitor (**Fig. 4D**). Though, apoptosis was not induced in UC, RCC, and PC cells 24 hours after treatment (**Fig. 4C**).

Figure 5.

Treatment effects of dual inhibitor (LAK-FFK11) *in vitro*. **A,** A PCA illustrating changes in chromatin accessibility upon treatment with LAK31, romidepsin, quisinostat, and LAK-FFK11 in comparison to the DMSO control as measured by ATAC-seq. **B,** A bar plot illustrating the number of opened (green) and closed (red) chromatin regions after treatment with the dual inhibitor LAK-FFK11 in 2102EP cells in comparison with DMSO solvent control. **C,** A HOMER algorithm-based screening for transcription factor–binding motifs in DNA rendered accessible or inaccessible after HDACi treatment of 2102EP cells. Venn diagrams summarize similarities in the identified TOP50 motifs. Bar diagrams highlight the TOP10 binding motifs (sorted by *P* value in LAK-FFK11–treated 2102EP cells) and their distribution in target sequences affected by HDACi treatment. Motifs identified in both, LAK-FFK11, and the other HDACi are labeled in green. **D,** A Volcano plot of transcriptional changes upon LAK-FFK11 treatment in comparison with the DMSO solvent control in 2102EP cells as measured by RNA-seq (FDR-corrected $P < 0.05$, FC $< -\log_2 2$ is shown in red; FC $> \log_2 2$ is shown in green). DAVID (**E**) and STRING (**F**) interaction analysis for commonly up- and downregulated genes of 2102EP cells treated with LAK-FFK11 (high stringency).

In addition, the MPAF fibroblasts remained unaffected regarding apoptosis and cell cycle alterations after application of high inhibitor concentrations (**Fig. 4C** and **E**; Supplementary Data S1E).

The molecular effects induced by the dual inhibitors found by qRT-PCR analysis (increased expression of *GADD45B, DUSP1, DHRS2* (HDACi-associated); decreased expression of *OCT3/4, GDF3* (BETi-associated) confirmed the multi-substrate activity in the tested GCT cells (TCam-2, 2102EP, GCT-72, and JAR; **Fig. 4F**).

To further elucidate the molecular effects upon treatment with the dual inhibitor LAK-FFK11, ATAC-, and RNA-seq of LAK-FFK11–treated 2102EP cells have been performed to evaluate DNA accessibility and transcriptome-wide changes, respectively (Supplementary Data S2T and S2U). A PCA revealed a separation of 2102EP cells treated with the dual inhibitor LAK-FFK11 from HDACi- (Romidepsin, Quisinostat, and LAK31) or DMSO treated 2102EP cells (**Fig. 5A**). As for the tested HDACi, on a global level LAK-FFK11 treatment caused an increase and decrease in DNA accessibility (**Fig. 5B**; Supplementary Figs. S5 and S6A, S6D, outer circle). We also screened for transcription factor–binding motifs affected by DNA accessibility after dual inhibitor treatment and compared the dual inhibitor with the other HDACi used in this study (**Fig. 5C**). The dual inhibitor showed a considerable overlap to the HDACi LAK31, Quisinostat and Romidepsin regarding the TOP50 identified motifs (24 shared motifs in accessible DNA and 33 in inaccessible DNA; **Fig. 5C**). In addition, the TOP10 motifs were highly similar to the motifs identified in HDACi (**Fig. 2E**, labeled in green).

Next, transcriptional changes have been analyzed upon LAK-FFK11 treatment in 2102EP (FC $\pm$ $\log_2$1.5, $P < 0.05$, 3,799 upregulated and 4,665 downregulated genes; **Fig. 5D**). Similar to our previous observations regarding transcriptional changes upon LAK31 treatment (**Fig. 3C** and **D**), the gene ontology analysis of the upregulated genes (FC > $\log_2$ 4, FDR-corrected $P < 0.05$) as well as STRING interaction analysis revealed an increase in gene sets related to regulation of differentiation, such as neurogenesis, which is in line with the upregulation of neuronal-associated genes after HDACi treatment in urological malignancies (**Fig. 5E** and **F**; Supplementary Fig. S7A). In addition, genes coding for histones were increased (**Fig. 5F**). A cluster of pluripotency and SMAD/NODAL signaling factors (*NANOG*, *NODAL*, *LEFTY1/2*, and *GDF3)* were significantly downregulated upon treatment with LAK-FFK11 (FC < $-\log_2$ 4, FDR-corrected $P < 0.05$; **Fig. 5F**).

Next, we compared and correlated changes in DNA accessibility and gene expression in 2102EP treated with either the HDACi LAK31 or the dual inhibitor LAK-FFK11 (Supplementary Fig. S6D). In addition, the Pearson correlation coefficient indicated a high correlation between both epi-drugs on transcriptome ($r = 0.876$) and DNA accessibility level ($r = 0.868$; Supplementary Fig. S6E).

We asked whether the epi-drugs affect sensitivity of cisplatin-resistant EC cells (2102EP-R, NCCIT-R, NT2/D1-R) toward cisplatin. Therefore, we combined treatment with either ASK44, LAK31, or LAK-FFK11 with cisplatin, but detected only slight additive effects in resistant GCT cells with regard to relative cell viability (Supplementary Data S1F).

Finally, we asked whether dual inhibitors were able to reduce tumor burden *in vivo*. Therefore, we xenografted 2102EP ($n = 7$) and the corresponding cisplatin-resistant subline 2102EP-R ($n = 8$) into the flank of nude mice and allowed tumors to grow for two weeks. Afterwards, we applied LAK-FFK11 (10 mg/kg) subcutaneously every second day for 21 days in total (**Fig. 6A**–**D**). A control group of mice were treated with the solvent DMSO. A measurement of the tumor volume demonstrated a significantly reduced tumor burden in dual inhibitor treated mice compared with the solvent-treated mice in both, 2102EP and 2102EP-R cells (**Fig. 6C** and **D**). During application, no considerable changes in mice's body weights were observed, pointing at a well-tolerated therapy (**Fig. 6E** and **F**). Histologically, the hematoxylin–eosin stainings show tumor cells with a solid growth pattern. The treated tumor cells show significant cell and nuclear pleomorphism in the form of a shifted nuclear/plasma relation. Necrosis can be seen between the vital tumor cells (**Fig. 6G** and **H**).

Discussion

In this study, we demonstrated the potential of novel HDACi and BETi as well as dual inhibitor approaches to treat (cisplatin-resistant) GCTs as well as UC, RCC and PC (**Fig. 6I** and **J**).

After screening 33 novel epi-drugs, we selected potent HDACi (KSK64, LAK31, and MPK409) and BETi (ASK44, ASK58, and ASK62) for extensive analysis and used them for the fusion into dual inhibitors (LAK-FFK11, LAK129, and LAK-HGK7; **Fig. 6I**). In comparison with other established HDACi and BETi, the novel epi-drugs demonstrated an increased efficacy in most GCT cell lines, whereas non-cancerous fibroblasts and keratinocytes presented as less sensitive toward the new epi-drugs, opening a potential therapeutic window. Nevertheless, immune cells (T-lymphocytes, monocytes) and endothelial cells were quite as sensitive as the GCT cells toward the individual HDACi and BETi, arguing for side-effects on these cell types during therapy, which need to be analyzed in detail in future studies. Regarding the dual inhibitors, fibroblasts, keratinocytes and T-lymphocytes and in parts endothelial cells (2 of 3 dual inhibitors) and monocytes (1 of 3 dual inhibitors) were less sensitive compared with the GCT cells. In addition, fibroblasts showed neither alterations in apoptosis rates nor the cell cycle phase distribution after dual inhibitor application. These data imply a reduced toxicity of the dual inhibitors to non-cancerous cells.

Earlier studies of HDACi observed an accumulation of cells in the G_2–M phase of the cell cycle, accompanied by apoptosis induction (21). The novel HDACi also induced apoptosis in GCT, UC and PC cell lines in comparison with the solvent control and accumulation in either G_1–G_0 or G_2–M cell cycle phase in a cell line-dependent manner (**Fig. 6I**). A BETi JQ1 treatment of GCT cell lines induced G_0–G_1 phase accumulation and apoptosis (17). The novel BETi also induced apoptosis in most GCT and PC cell lines and predominantly led to accumulation of cells in G_1–G_0 phase (**Fig. 6I**). The three dual inhibitors induced apoptosis in GCT cell lines, but failed to trigger apoptosis in UC, PC and RCC cell lines. Regarding UC, this was a rather unexpected finding as combinatorial treatment with the BETi JQ1 and the HDACi Romidepsin has been shown to exceed synergistic antineoplastic efficacy in UC cell lines (18). Xenotransplantations in mice have proven the potential of the dual inhibitor LAK-FFK11 to reduce GCT growth *in vivo*, while having no effect on mice's body weight. Even though the BET component JQ1 has been previously proven to be 49% orally bioavailable (14), further research has to be conducted regarding the oral bioavailability of LAK-FFK11. In comparison with earlier published HDAC-BET-dual inhibitors (55, 56) the novel LAK-FFK11 displayed a higher affinity toward BRDs and HDACs (Supplementary Fig. S4E and S4F), while remaining a low toxicity in *in vitro* and *in vivo* experiments. In summary, the dual inhibitors predominantly present as therapeutic options for (cisplatin-resistant) GCTs, whereas the HDACi and BETi individually are suitable therapeutics for all tested urological malignancies.

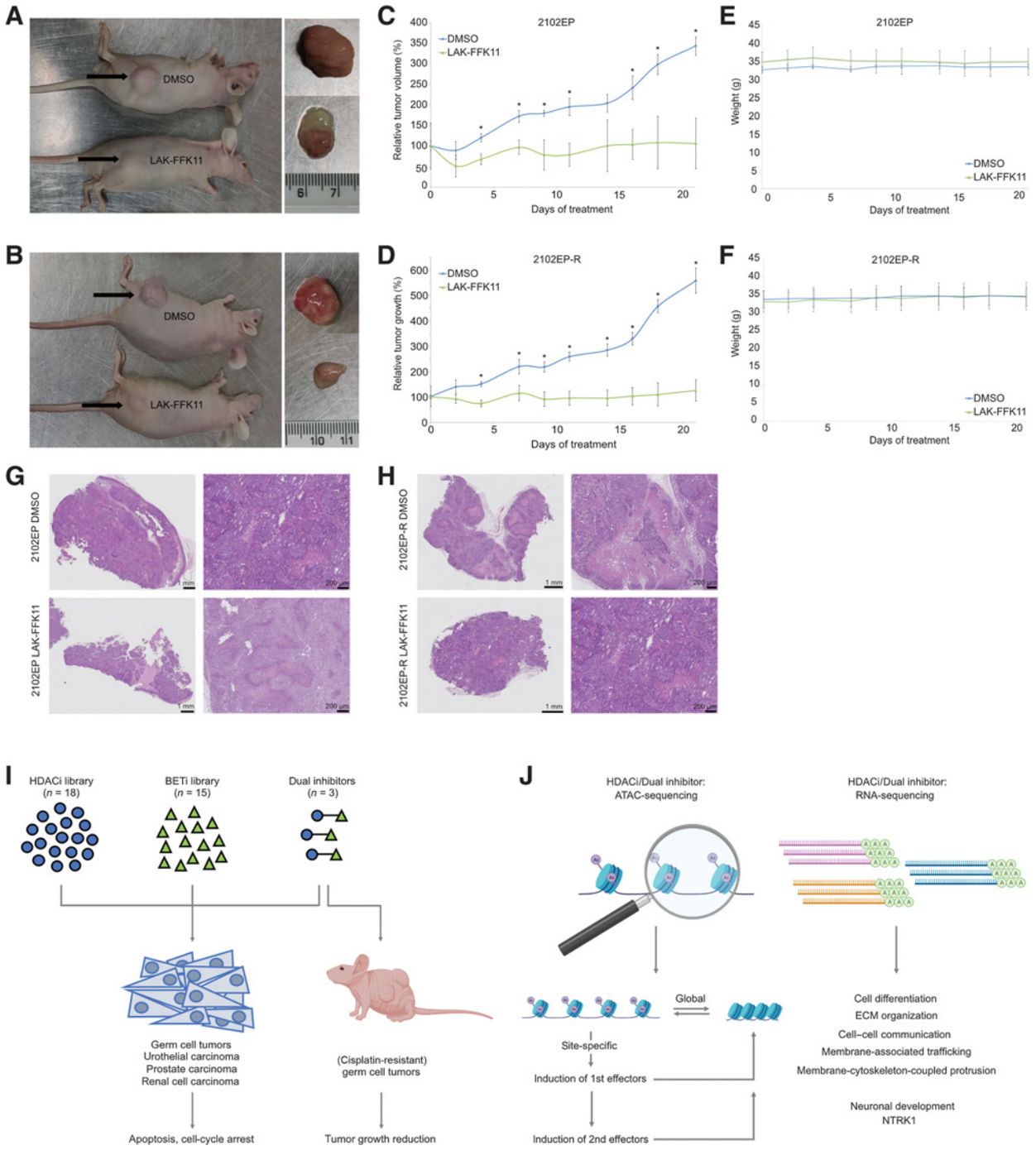

Figure 6.

Treatment effects of dual inhibitor (LAK-FFK11) on xenotransplanted 2102EP(-R). Macroscopic appearance of DMSO and LAK-FFK11 treated 2102EP (**A**) and 2102EP-R (**B**) xenografted tumors. *In vivo* results of tumor growth inhibition by LAK-FFK11 in xenografted 2102EP (**C**) and 2102EP-R (**D**) cells. The relative tumor volume is displayed over a period of 3 weeks. Treatment and measurements were performed every 2 days. Weight of mice has been examined in xenografted 2102EP (**E**) and 2102EP-R (**F**) cells treated with either LAK-FFK11 or solvent control. Hematoxylin–eosin (H&E) staining of DMSO and LAK-FFK11 treated 2102EP (**G**) and 2102EP-R (**H**) xenografted tumors. Graphical summary the key findings of this study (**I**) and molecular effects of HDACi/dual inhibition (**J**).

On a molecular level and in line with other HDACi studies, LAK31 treatment led to a strongly increased gene expression in all four analyzed tumor cell lines (21, 57–62). The novel HDACi LAK31, KSK64, and MPK409 function in a similar way as Romidepsin, proven by upregulation of cell cycle and apoptosis regulators (e.g., *ATF3, DUSP1, FOS*, and *GADD45B*) in all four tumor entities (22, 53). *DHRS2* was strongly upregulated in all studied GCT, UC, PC and RCC cell lines after HDACi (LAK31 and Romidepsin) treatment, further manifesting its status as a pan-marker of a successful HDACi treatment in urological malignancies (21, 37). Gene expression alterations after treatment with BETi ASK44, ASK58, and ASK62 were similar to JQ1, such as the downregulation of the pluripotency gene (*OCT3/4)* and the TGF-β ligand *GDF3* as well as upregulation of stress response and cell cycle regulators (*ATF3* and *CDKN1C)* in three of the four tested cell lines (17). Thus, on a molecular level, the effects on key factors after application of the newly synthesized and established HDACi/BETi were quite similar, arguing that alterations in these factors reflect a general response to HDACi and BETi.

When comparing the molecular functions related to the upregulated genes after HDACi application in all studied urological malignancies, we found that these genes could be linked to the extracellular matrix, intra- and extracellular membrane-associated trafficking and cell–cell communication as well as to membrane–cytoskeleton-coupled protrusion (**Fig. 6J**). In conclusion, HDACi affect mobility, communication, molecule trafficking, and microenvironment interactions of treated tumor cells. In addition, 14 genes associated with neuronal development and differentiation were upregulated after HDACi application (*CHRM4*, *DNAH2*, *DNER*, *DPYSL4*, *GIPR*, *GRIN1*, *LHX9*, *NCAM1*, *NDNF*, *NRXN2*, *NTRK1*, *NYAP1*, *PTGER3*, and *SYP*; Supplementary Fig. S7A). Upregulation of *NTRK1* by LAK31 has been confirmed by qRT-PCR in 3 of 4 GCT cell lines (Supplementary Fig. S7F, left). Similarly, treatment with the dual inhibitor LAK-FFK11 resulted in elevated *NTRK1* expression in 2102EP (Supplementary Fig. S7F, right). Generally, neuronal differentiation in GCTs is not associated with a poor prognosis, except for the presence of neuroectodermal-differentiated cell populations, which is indeed linked to a worse prognosis. This is also true in PC, in which neuroendocrine differentiation triggered by continuous androgen deprivation significantly impairs patients' outcome and prognosis (63). In line, two upregulated neuronal genes (*NCAM1* and *SYP*) were associated with "neuroendocrine carcinoma" (Supplementary Fig. S7A). Thus, induction of neuronal-associated genes and related developmental processes might be a risk of HDACi, if differentiation into neuroendocrine lineage occurs, and clarifies the need for carefully adjusting the concentrations applied during therapy, that is, high enough to rapidly kill tumor cells and avoid neuroendocrine differentiation, but low enough to circumvent severe global side-effects.

It is generally acknowledged that HDACi induce hyperacetylation of histones, which is associated with "accessible" DNA. Thus, LAK31 treatment was expected to strongly increase levels of DNA accessibility. Interestingly, in urological malignancies treatment with novel (LAK31) and established (Romidepsin and Quisinostat) HDACi did not only increase the global chromatin accessibility, but also led to reduced DNA accessibility. In fact, levels of "closed" DNA regions were similar to even higher compared with DNA accessibility after HDACi application (LAK31, ratio DNA accessibility: 2102EP = 0.91, VM-CUB-1 = 0.59, Caki-1 = 0.35, DU-145 = 0.52; Romidepsin: 2102EP = 0.82; Quisinostat: 2102EP = 0.82; **Figs. 2B** and **D**, and **6J**). In line, in a previous publication a pan-H3ac-ChIP-seq analysis of TCam-2 treated with the HDACi Romidepsin found decreased H3ac levels in gene bodies, promotors and active regions, whereas a global enrichment could be observed in regions ± 5 kilobases upstream or downstream of the gene bodies and promotors (22). In summary, HDACi seem to cause a global increase in histone acetylation, but mainly in non-gene body and non-promotor context, resulting in a decreased chromatin accessibility in gene bodies and promotors.

Nevertheless, we also observed site-specific chromatin openings, which correlated to increasing gene expression (**Fig. 6J**). The number of upregulated genes was considerably higher than the number of downregulated genes (LAK31, ratio up- to downregulated genes: 2102EP = 6.09; VM-CUB-1 = 2.93, Caki-1 = 2.34, DU-145 = 2.31; **Fig. 3A**).

Thus, the changes in chromatin accessibility do not reflect the high number of upregulated genes and low number of downregulated genes. Therefore, we hypothesize that in first-line, an HDACi induced site-specific chromatin opening results in a direct upregulation of a set of factors feedbacking on the epigenetic landscape, causing (i) a closing of certain chromatin regions and (ii) inducing a considerable number of second-line factors, that is, epigenetic modifiers, which might influence chromatin accessibility (**Fig. 6J**). To our knowledge, this study is the first to question the paradigm that HDACi solely lead to enhanced DNA accessibility. However, the underlying mechanisms need to be studied further, because this finding could change the fundamental understanding of the HDACi mode of action.

We identified three genes/loci commonly altered in expression and chromatin accessibility after HDACi application in all tested cell lines of urological origin (upregulated/opened: *TEX14*; downregulated/closed: *KIRREL, MARVELD1*; Supplementary Fig. S7E). *TEX14* is a germ cell (tumor)–associated gene required for the formation of intercellular bridges during meiosis and for kinetochore–microtubule attachment during mitosis in cooperation with PLK1 (64–66). In GCTs, *TEX14* was classified as a GCT predisposition loci (67, 68). According to the "The Human Protein Atlas," *KIRREL* and *MARVELD1* (but not *TEX14*) are prognostic markers of poor prognosis in UC, RCC and cervical cancer as well as RCC and lung cancer, respectively (Supplementary Fig. S7G; ref. 50). Thus, downregulation of *KIRREL* and *MARVELD1* expression after HDACi treatment, accompanied by chromatin closing at corresponding loci, might be beneficial for the overall prognosis.

Further transcriptome-wide analysis of the dual inhibitor confirmed that the mode of action of the HDACi-component was similar to LAK31 (**Fig. 5D–F**). Moreover, treatment with the dual inhibitor resulted in a high redundancy to HDACi treated (LAK31, Quisinostat, and Romidepsin) 2102EP cells regarding affected transcription factor–binding motifs (**Fig. 5C**). Especially, the previously mentioned elevated neuronal-associated and developmental gene sets should be carefully taken into consideration upon application of the drug to circumvent neuroendocrine differentiation (Supplementary Fig. S7F).

In summary, this study provides novel HDAC and BET mono inhibitors as treatment options for urological malignancies, including cisplatin-resistant GCTs. Fusion of HDACi and BETi into a dual inhibitor showed promising results in reducing cell viability especially in GCTs *in vitro* and *in vivo*, while being less efficient in non-malignant cells. In addition, we identified epigenetic and molecular mechanisms commonly altered by HDACi in urological malignancies, leading to a better understanding of the modes-of-action of the drugs during therapy.

Authors' Disclosures

F. Fischer reports personal fees from Research Training Group GRK 2158 and Deutsche Forschungsgemeinschaft (DFG, German Research Foundation) during the conduct of the study. G. Niegisch reports personal fees from Roche Pharma, MEDAC, Pfizer, BMS, AstraZeneca, Sanofi, Ipsen, Janssen, and Merck outside the submitted work. M.A. Skowron reports grants from Forschungskommission (FoKo) der Medizinischen Fakultt der Heinrich-Heine-Universit Dseldorf, Germany, during the

conduct of the study; MZ1 has been provided for free by Boehringer Ingelheim International via https://opnme.com/. D. Nettersheim reports grants from Dr. K. und B. Wegener-Stiftung during the conduct of the study. No disclosures were reported by the other authors.

Authors' Contributions

A. Burmeister: Data curation, software, formal analysis, validation, investigation, visualization, writing–original draft. **A. Stephan:** Data curation, formal analysis, validation, investigation. **L.A. Alves Avelar:** Data curation, formal analysis, investigation, visualization, writing–original draft. **M.R. Müller:** Data curation, validation, investigation. **A. Seiwert:** Resources. **S. Höfmann:** Resources. **F. Fischer:** Resources. **H. Torres-Gomez:** Resources. **M.J. Hoffmann:** Investigation, writing–review and editing. **G. Niegisch:** Investigation. **F. Bremmer:** Writing–review and editing. **P. Petzsch:** Software, formal analysis, investigation, visualization. **K. Köhrer:** Resources, methodology. **P. Albers:** Resources, project administration, writing–review and editing. **T. Kurz:** Conceptualization, resources, supervision, methodology, writing–review and editing. **M.A. Skowron:** Conceptualization, resources, data curation, software, formal analysis, supervision, funding acquisition, validation, investigation, visualization, methodology, writing–original draft, project administration. **D. Nettersheim:** Conceptualization, resources, data curation, formal analysis, supervision, funding acquisition, visualization, methodology, writing–original draft, project administration, writing–review and editing.

Acknowledgments

We kindly thank Anna Pehlke for excellent technical assistance. We kindly thank Dr. Michal Mego, Dr. Matthew J. Murray, Dr. Petra Boukamp, Dr. Rüdiger Sorg, Dr. Victoria Kolb-Bachofen, Dr. Gerhard Fritz, Dr. Michael Peitz, Dr. Christoph Oing, and Dr. Thomas Müller for providing GCT cell lines and healthy control cells (see Supplementary Table S1A). We thank the initiative opn.me (https://opnme.com) by Boehringer Ingelheim for providing MZ-1 for free. In addition, we would like to thank the Active Motif team, especially Matthias Spiller-Becker, for excellent technical support. F. Bremmer is supported by the Wilhelm Sander-Stiftung (grant numbers 2016.041.1, 2016.041.2 and 2016.041.3). We thank Olga Dschun for excellent technical assistance. This study has been performed as part of the "Lighthouse Project Germ Cell Tumors" of the "Centre for Integrated Oncology—Aachen, Bonn, Cologne, Düsseldorf" (CIO^{ABCD}). This study was supported by the "Forschungskommission (FoKo) der Medizinischen Fakultät der Heinrich-Heine-Universität Düsseldorf (2019–24; to M.A. Skowron) and the Brigitte und Dr. Konstanze Wegener-Stiftung (#36; to D. Nettersheim). The authors would like to thank the Deutsche Forschungsgemeinschaft (DFG) and the Research Training Group GRK 2158 for funding (to T. Kurz).

The publication costs of this article were defrayed in part by the payment of publication fees. Therefore, and solely to indicate this fact, this article is hereby marked "advertisement" in accordance with 18 USC section 1734.

Note

Supplementary data for this article are available at Molecular Cancer Therapeutics Online (http://mct.aacrjournals.org/).

Received March 24, 2022; revised July 18, 2022; accepted August 15, 2022; published first August 23, 2022.

References

1. Sung H, Ferlay J, Siegel RL, Laversanne M, Soerjomataram I, Jemal A, et al. Global cancer statistics 2020: GLOBOCAN estimates of incidence and mortality worldwide for 36 cancers in 185 countries. CA Cancer J Clin 2021;71:209–49.
2. Park JS, Kim J, Elghiaty A, Ham WS. Recent global trends in testicular cancer incidence and mortality. Medicine 2018;97:e12390.
3. Berney DM, Looijenga LHJ, Idrees M, Oosterhuis JW, Rajpert-De Meyts E, Ulbright TM, et al. Germ cell neoplasia in situ (GCNIS): evolution of the current nomenclature for testicular pre-invasive germ cell malignancy. Histopathology 2016;69:7–10.
4. Oosterhuis JW, Looijenga LHJ. Testicular germ-cell tumours in a broader perspective. Nat Rev Cancer 2005;5:210–22.
5. Oing C, Giannatempo P, Honecker F, Oechsle K, Bokemeyer C, Beyer J. Palliative treatment of germ cell cancer. Cancer Treat Rev 2018;71:102–7.
6. Patel VG, Oh WK, Galsky MD. Treatment of muscle-invasive and advanced bladder cancer in 2020. CA Cancer J Clin 2020;70:404–23.
7. Reesink DJ, van de Garde EMW, Peters BJM, van der Nat PB, Los M, Horenblas S, et al. Treatment patterns and clinical outcomes of chemotherapy treatment in patients with muscle-invasive or metastatic bladder cancer in the Netherlands. Sci Rep 2020;10:15822.
8. Tosoian JJ, Mamawala M, Epstein JI, Landis P, Wolf S, Trock BJ, et al. Intermediate and longer-term outcomes from a prospective active-surveillance program for favorable-risk prostate cancer. J Clin Oncol 2015;33:3379–85.
9. Koo KC, Park SU, Kim KH, Rha KH, Hong SJ, Yang SC, et al. Prognostic impacts of metastatic site and pain on progression to castrate resistance and mortality in patients with metastatic prostate cancer. Yonsei Med J 2015;56:1206–12.
10. Grimm MO, Wolff I, Zastrow S, Fröhner M, Wirth M. Advances in renal cell carcinoma treatment. Ther Adv Urol 2010;2:11–7.
11. Von Der Maase H, Sengelov L, Roberts JT, Ricci S, Dogliotti L, Oliver T, et al. Long-term survival results of a randomized trial comparing gemcitabine plus cisplatin, with methotrexate, vinblastine, doxorubicin, plus cisplatin in patients with bladder cancer. J Clin Oncol 2005;23:4602–8.
12. Skowron MA, Melnikova M, Van Roermund JGH, Romano A, Albers P, Thomale J, et al. Multifaceted mechanisms of cisplatin resistance in long-term treated urothelial carcinoma cell lines. Int J Mol Sci 2018;19:590.
13. Ganesan A, Arimondo PB, Rots MG, Jeronimo C, Berdasco M. The timeline of epigenetic drug discovery: from reality to dreams. Clin Epigenetics 2019;11:174.
14. Filippakopoulos P, Qi J, Picaud S, Shen Y, Smith WB, Fedorov O, et al. Selective inhibition of BET bromodomains. Nature 2010;468:1067–73.
15. Bennett RL, Licht JD. Targeting epigenetics in cancer. Annu Rev Pharmacol Toxicol 2018;58:187–207.
16. Sahai V, Redig AJ, Collier KA, Eckerdt FD, Munshi HG. Targeting bet bromodomain proteins in solid tumors. Oncotarget 2016;7:53997–4009.
17. Jostes S, Nettersheim D, Fellermeyer M, Schneider S, Hafezi F, Honecker F, et al. The bromodomain inhibitor JQ1 triggers growth arrest and apoptosis in testicular germ cell tumours in vitro and in vivo. J Cell Mol Med 2017;21:1300–14.
18. Holscher AS, Schulz WA, Pinkerneil M, Niegisch G, Hoffmann MJ. Combined inhibition of BET proteins and class I HDACs synergistically induces apoptosis in urothelial carcinoma cell lines. Clin Epigenetics 2018;10:1.
19. Bai Y, Ahmad D, Wang T, Cui G, Li W. Research advances in the use of histone deacetylase inhibitors for epigenetic targeting of cancer. Curr Top Med Chem 2019;19:995–1004.
20. Autin P, Blanquart C, Fradin D. Epigenetic drugs for cancer and microRNAs: a focus on histone deacetylase inhibitors. Cancers 2019;11:1530.
21. Nettersheim D, Berger D, Jostes S, Skowron M, Schorle H. Deciphering the molecular effects of romidepsin on germ cell tumours: DHRS2 is involved in cell cycle arrest but not apoptosis or induction of romidepsin effectors. J Cell Mol Med 2019;23:670–9.
22. Nettersheim D, Jostes S, Fabry M, Honecker F, Schumacher V, Kirfel J, et al. A signaling cascade including ARID1A, GADD45B and DUSP1 induces apoptosis and affects the cell cycle of germ cell cancers after romidepsin treatment. Oncotarget 2016;7:74931–46.
23. Paillas S, Then CK, Kilgas S, Ruan JL, Thompson J, Elliott A, et al. The histone deacetylase inhibitor romidepsin spares normal tissues while acting as an effective radiosensitizer in bladder tumors in vivo. Int J Radiat Oncol Biol Phys 2020;107:212–21.
24. Pattarawat P, Hong T, Wallace S, Hu Y, Donnell R, Wang TH, et al. Compensatory combination of romidepsin with gemcitabine and cisplatin to effectively and safely control urothelial carcinoma. Br J Cancer 2020;123:226–39.
25. Zhang Z, Hou S, Chen H, Ran T, Jiang F, Bian Y, et al. Targeting epigenetic reader and eraser: rational design, synthesis and in vitro evaluation of dimethylisoxazoles derivatives as BRD4/HDAC dual inhibitors. Bioorg Med Chem Lett 2016;26:2931–5.
26. Anighoro A, Bajorath J, Rastelli G. Polypharmacology: challenges and opportunities in drug discovery. J Med Chem 2014;57:7874–87.
27. Medina-Franco JL, Giulianotti MA, Welmaker GS, Houghten RA. Shifting from the single to the multitarget paradigm in drug discovery. Drug Discov Today 2013;18:495–501.

28. Alves LA, Schrenk C, Melf S, Hamacher A, Hansen FK, Schliehe-Diecks J, et al. Synergistic induction of apoptosis in resistant head and neck carcinoma and leukemia by alkoxyamide-based histone deacetylase inhibitors. Eur J Med Chem 2021;211:113095.
29. Asfaha Y, Schrenk C, Alves Avelar LA, Lange F, Wang C, Bandolik JJ, et al. Novel alkoxyamide-based histone deacetylase inhibitors reverse cisplatin resistance in chemoresistant cancer cells. Bioorganic Med Chem 2020;28:115108.
30. Stenzel K, Hamacher A, Hansen FK, Gertzen CGW, Senger J, Marquardt V, et al. Alkoxyurea-based histone deacetylase inhibitors increase cisplatin potency in chemoresistant cancer cell lines. J Med Chem 2017;60:5334–48.
31. Pflieger M, Hamacher A, Öz T, Horstick-Muche N, Boesen B, Schrenk C, et al. Novel α,β-unsaturated hydroxamic acid derivatives overcome cisplatin resistance. Bioorganic Med Chem 2019;27:115036.
32. Marek L, Hamacher A, Hansen FK, Kuna K, Gohlke H, Kassack MU, et al. Histone deacetylase (HDAC) inhibitors with a novel connecting unit linker region reveal a selectivity profile for HDAC4 and HDAC5 with improved activity against chemoresistant cancer cells. J Med Chem 2013;56:427–36.
33. Pflieger M, Sönnichsen M, Horstick-Muche N, Yang J, Schliehe-Diecks J, Schöler A, et al. Oxa analogues of nexturastat A demonstrate improved HDAC6 selectivity and superior anti-leukaemia activity. ChemMedChem 2021;16:1799–804.
34. Dong J, Wang NN, Yao ZJ, Zhang L, Cheng Y, Ouyang D, et al. ADMETlab: a platform for systematic ADMET evaluation based on a comprehensively collected ADMET database. J Cheminform 2018;10:29.
35. Xiong G, Wu Z, Yi J, Fu L, Yang Z, Hsieh C, et al. ADMETlab 2.0: an integrated online platform for accurate and comprehensive predictions of ADMET properties. Nucleic Acids Res 2021;49:W5–14.
36. Skowron MA, Becker TK, Kurz L, Jostes S, Bremmer F, Fronhoffs F, et al. The signal transducer CD24 suppresses the germ cell program and promotes an ectodermal rather than mesodermal cell fate in embryonal carcinomas. Mol Oncol 2022;16:982–1008.
37. Kurz L, Miklyaeva A, Skowron MA, Overbeck N, Poschmann G, Becker T, et al. ARID1A regulates transcription and the epigenetic landscape via POLE and DMAP1 while ARID1A deficiency or pharmacological inhibition sensitizes germ cell tumor cells to ATR inhibition. Cancers 2020;12:905.
38. Fichtner A, Richter A, Filmar S, Gaisa NT, Schweyer S, Reis H, et al. The detection of isochromosome i(12p) in malignant germ cell tumours and tumours with somatic malignant transformation by the use of quantitative real-time polymerase chain reaction. Histopathology 2021;78:593–606.
39. Goldman MJ, Craft B, Hastie M, Repečka K, McDade F, Kamath A, et al. Visualizing and interpreting cancer genomics data via the Xena platform. Nat Biotechnol 2020;38:675–8.
40. Gao J, Aksoy BA, Dogrusoz U, Dresdner G, Gross B, Sumer SO, et al. Integrative analysis of complex cancer genomics and clinical profiles using the cBioPortal. Sci Signal 2013;6:pl1.
41. Cerami E, Gao J, Dogrusoz U, Gross BE, Sumer SO, Aksoy BA, et al. The cBio Cancer Genomics Portal: an open platform for exploring multidimensional cancer genomics data. Cancer Discov 2012;2:401–4.
42. Heberle H, Meirelles VG, da Silva FR, Telles GP, Minghim R. InteractiVenn: a web-based tool for the analysis of sets through Venn diagrams. BMC Bioinf 2015;16:169.
43. Szklarczyk D, Gable AL, Lyon D, Junge A, Wyder S, Huerta-Cepas J, et al. STRING v11: protein–protein association networks with increased coverage, supporting functional discovery in genome-wide experimental datasets. Nucleic Acids Res 2019;47:D607–13.
44. Huang DW, Sherman BT, Lempicki RA. Systematic and integrative analysis of large gene lists using DAVID bioinformatics resources. Nat Protoc 2009;4:44–57.
45. Heinz S, Benner C, Spann N, Bertolino E, Lin YC, Laslo P, et al. Simple combinations of lineage-determining transcription factors prime cis-regulatory elements required for macrophage and B-cell identities. Mol Cell 2010;38:576–89.
46. Yu Y, Ouyang Y, Yao W. shinyCircos: an R/Shiny application for interactive creation of Circos plot. Bioinformatics 2018;34:1229–31.
47. Gerst R, Olzer MH. PCAGO: an interactive web service to analyze RNA-Seq data with principal component analysis. BioRxiv. Available from: https://www.biorxiv.org/content/10.1101/433078v3.
48. Hunter JD. Matplotlib: a 2D graphics environment. Comput Sci Eng 2007;9:90–5.
49. Waskom ML. Seaborn: statistical data visualization. J Open Source Softw 2021;6:3021.
50. Uhlén M, Fagerberg L, Hallström BM, Lindskog C, Oksvold P, Mardinoglu A, et al. Tissue-based map of the human proteome. Science 2015;347:1260419.
51. Hu E, Dul E, Sung CM, Chen Z, Kirkpatrick R, Zhang GF, et al. Identification of novel isoform-selective inhibitors within class I histone deacetylases. J Pharmacol Exp Ther 2003;307:720–8.
52. Tang R, Li Y, Han F, Li Z, Lin X, Sun H, et al. A CTCF-binding element and histone deacetylation cooperatively maintain chromatin loops, linking to long-range gene regulation in cancer genomes. Front Oncol 2022;11:821495.
53. Pinkerneil M, Hoffmann MJ, Deenen R, Köhrer K, Arent T, Schulz WA, et al. Inhibition of class I histone deacetylases 1 and 2 promotes urothelial carcinoma cell death by various mechanisms. Mol Cancer Ther 2016;15:299–312.
54. Zhou S, Zhang S, Wang L, Huang S, Yuan Y, Yang J, et al. BET protein inhibitor JQ1 downregulates chromatin accessibility and suppresses metastasis of gastric cancer via inactivating RUNX2/NID1 signaling. Oncogenesis 2020;9:33.
55. Ren Q, Gao W. Current status in the discovery of dual BET/HDAC inhibitors. Bioorg Med Chem Lett 2021;38:127829.
56. Zhang X, Zegar T, Weiser T, Hamdan FH, Berger BT, Lucas R, et al. Characterization of a dual BET/HDAC inhibitor for treatment of pancreatic ductal adenocarcinoma. Int J Cancer 2020;147:2847–61.
57. Slaughter MJ, Shanle EK, Khan A, Chua KF, Hong T, Allis CD, et al. HDAC inhibition results in widespread alteration of the histone acetylation landscape and BRD4 targeting to gene bodies. Cell Rep 2021;34:108638.
58. Wang Z, Zang C, Cui K, Schones DE, Barski A, Peng W, et al. Genome-wide mapping of HATs and HDACs reveals distinct functions in active and inactive genes. Cell 2009;138:1019.
59. Kaletsch A, Pinkerneil M, Hoffmann MJ, Jaguva Vasudevan AA, Wang C, Hansen FK, et al. Effects of novel HDAC inhibitors on urothelial carcinoma cells. Clin Epigenetics 2018;10:100.
60. Xu WS, Parmigiani RB, Marks PA. Histone deacetylase inhibitors: molecular mechanisms of action. Oncogene 2007;26:5541–52.
61. Ruscetti M, Dadashian EL, Guo W, Quach B, Mulholland DJ, Park JW, et al. HDAC inhibition impedes epithelial–mesenchymal plasticity and suppresses metastatic, castration-resistant prostate cancer. Oncogene 2016;35:3781–95.
62. Chueh AC, Tse JWT, Tögel L, Mariadason JM. Mechanisms of histone deacetylase inhibitor-regulated gene expression in cancer cells. Antioxid Redox Signal 2015;23:66.
63. Conteduca V, Oromendia C, Eng KW, Bareja R, Sigouros M, Molina A, et al. Clinical features of neuroendocrine prostate cancer. Eur J Cancer 2019;121:7–18.
64. Wang PJ, McCarrey JR, Yang F, Page DC. An abundance of X-linked genes expressed in spermatogonia. Nat Genet 2001;27:422–6.
65. Kim HJ, Yoon J, Matsuura A, Na JH, Lee WK, Kim H, et al. Structural and biochemical insights into the role of testis-expressed gene 14 (TEX14) in forming the stable intercellular bridges of germ cells. Proc Natl Acad Sci U S A 2015;112:12372–7.
66. Mondal G, Ohashi A, Yang L, Rowley M, Couch FJ. Tex14, a Plk1-regulated protein, is required for kinetochore-microtubule attachment and regulation of the spindle assembly checkpoint. Mol Cell 2012;45:680–95.
67. Ruark E, Seal S, McDonald H, Zhang F, Elliot A, Lau K, et al. Identification of nine new susceptibility loci for testicular cancer, including variants near DAZL and PRDM14. Nat Genet 2013;45:686–9.
68. Pyle LC, Nathanson KL. Genetic changes associated with testicular cancer susceptibility. Semin Oncol 2016;43:575–81.